M. Sicard, C. Pérez, F. Rocadenbosch, J.M. Baldasano, D. Garcia-Vizcaino (2005) **Mixed layer depth determination in the Barcelona costal area from regular lidar measurements: methods, results and limitations.** Boundary-Layer Meteorology (in press)

Mixed layer depth determination in the Barcelona coastal area from regular lidar measurements: methods, results and limitations

M. Sicard[a], C. Pérez[b], F. Rocadenbosch[a], J.M. Baldasano[b], D. García-Vizcaino[a]

[a]Universitat Politècnica de Catalunya, Dept. de TSC, Jordi Girona 1, 08034 Barcelona, Spain

[b]Universitat Politècnica de Catalunya, LMA, Avda. Diagonal 647, planta 10, 08028 Barcelona, Spain

Corresponding author address: Michaël Sicard

UPC, Dept. of TSC

c/ Jordi Girona, 1, Edif. D4-010

08034 Barcelona, Spain

Telephone: (+34) 934 011 065

Fax: (+34) 934 017 200

Email: msicard@tsc.upc.edu

ABSTRACT

Regular aerosol backscatter measurements using an elastic-backscatter lidar were performed between May 2000 and December 2002 in Barcelona (Spain), in the frame of the European project EARLINET (European Aerosol Research Lidar Network). The mixed layer depth, required to understand the physical and chemical processes taking place in the low troposphere, was one of the major parameters to be retrieved. Three derivative methods have been tested in this complex coastal area using the range squared-corrected lidar signal: (1) the minimum of its first derivative, (2) the minimum of its second derivative, and (3) the minimum of the first derivative of its logarithm. The second method was found to give statistically the best results when compared to radiosoundings and it was used to process the whole dataset. A number of 162 days and 660 profiles averaged over 30 minutes have been examined. The mixed layer depth was inferred in cases such as Saharan dust events and sea breeze and mountain-induced re-circulations. It oscillates between 300 and 1450 m in summer and between 390 and 1420 m in winter from 1000 to 1500 UTC. The standard deviation for this portion of the day is 180 and 256 m, respectively in summer and winter. In summer, low heights (mainly limited to 400 - 800 m) are associated to large mesoscale compensatory subsidence over the sea and to the thermal internal boundary layer formation. The strong coastal and orographic influences and the climatological settling of Barcelona determine the complexity of its atmospheric boundary layer dynamics and the high heterogeneity of the lidar signals. In many cases, single lidar analyses do not allow an unambiguous determination of the mixed layer depth. Two diurnal cycle measurements are discussed together with synoptic maps, backtrajectories and radiosoundings in order to outline the complexity of the area and the limitations of the methods.

Keywords : mixed layer depth, lidar profiles, radiosoundings, complex terrain, coastal region

1. INTRODUCTION

The atmospheric boundary layer (ABL) can be defined as the part of the troposphere that is directly influenced by the presence of the earth's surface, and responds to surface forcings with a timescale of about an hour or less (Stull, 1988). The ABL thickness is quite variable in space and time, ranging from hundreds of meters to a few kilometres. It is usual in air pollution meteorology to use the term mixed layer (ML) since pollutants that are emitted into the ABL become gradually dispersed and mixed through the action of turbulence. The mixed layer depth (MLD) is the height of the top of the ML and is a key parameter to characterize its structure. In some papers, the MLD is also called the mixing height (Seibert et al., 1998; 2000). Measurements, parameterizations and predictions of the MLD have many theoretical and practical applications such as the prediction of pollutant concentrations and surface temperature, the scaling of turbulence measurements or the treatment of the ML in numerical weather prediction and climate models (Seibert et al., 1998). Different ways exist to determine or estimate the MLD. During daytime, radiosoundings are the most common data source to retrieve the MLD based on wind, temperature and pressure profiles but in most stations regular launches are made only twice a day at pre-determined synoptic times (0000 and 1200 UTC). Consequently, radiosoundings can often be used as a reference for comparison with modelled ABL heights only around midnight and noon.

Active remote sensing systems such as lidars use aerosols as tracers of the ABL dynamics. The optical power measured by a lidar device is proportional to the aerosol content of the atmosphere. The lidar signal shows a strong backscattering within the ML, which decreases through a transition zone and becomes weak in the free troposphere (FT). These contrasts are the basis for the lidar estimations of the MLD. Under convective conditions, the ABL can be divided into three different layers: the surface layer, the ML and the entrainment zone (EZ). The latter represents a transition zone between the ML and the stable FT above. Usually, the EZ is defined in a horizontal average sense (Deardorff et al, 1980). It is important to distinguish between the instantaneous (or local) MLD that varies between the EZ top and the middle of the ML and the average MLD which is the

middle of the EZ (Stull, 1988). Ground-based aerosol lidars give a high-resolution picture of the instantaneous ML top that is marked by a large contrast between the backscatter signal from aerosol-rich structures below and cleaner air above. This lidar transition zone should not be confused with the classical definition of EZ defined by Deardorff et al. (1980) given above. Furthermore, it is worth noting that the lidar-derived transition zone, usually assumed to correspond closely with the temperature inversion, does not respond directly to the thermodynamic properties of the atmosphere: it can only be assumed to be a proxy for the temperature inversion (Brooks, 2003).

However, interpreting data from lidars is often not straightforward, because the detected layers are not always the result of ongoing vertical mixing, but may originate from advective transport or past accumulation processes (Seibert et al., 2000). In our case, Barcelona is a coastal city located at the northeastern Iberian Peninsula (IP) and surrounded by complex orography. The meteorology and the origin of the air masses arriving at the IP are highly influenced by the Azores high-pressure system that is located over the Atlantic Ocean. The more usual synoptic situations affecting the Barcelona area are westerly and northwesterly flows in winter, and typical summertime weak pressure gradients (Martín-Vide, 1987; Jorba et al., 2004; Pérez et al., 2004). Under the latter conditions, mesoscale phenomena modify the ML flow generating circulations in conjunction with diurnal heating cycles. A thermal internal boundary layer (TIBL) forms and increases in depth to merge eventually with the ML at some distances from the coastline (Soriano et al., 2001). The nearby orography of the region shown in Figure 1 is dominated by four main features arranged parallel to the coastline: the coastal plain, the coastal mountain range (500 - 700 m), the pre-coastal depression, and the pre-coastal mountain range (700 - 1700 m). In summer, under strong insolation and weak synoptic forcing, sea breezes and mountain-induced winds develop to create re-circulations of pollutants along the eastern Iberian coast. Layers are formed when aerosols are injected from the mountains into the return flow at various heights and distances from the coast (Millán et al., 1997; Soriano et al., 2001; Barros et al., 2003; Pérez et al., 2004). In addition, the synoptic scale

meteorology induces frequent outbreaks of Saharan dust in summer (Rodríguez et al., 2001; Pérez et al., 2003).

Several approaches have been used to estimate the MLD from lidar. Melfi et al. (1985) and Boers et al. (1988) used simple signal threshold values. It suffers from the need to define them appropriately taking into account that the signal strength varies within the dataset. Hooper and Eloranta (1986) used the height of the maximum of the variance of the lidar signal. Some authors detected that the results tended to be biased to higher altitudes due to humidity effects (Dupont et al., 1991; Menut et al., 1999). Derivative methods are the most common. A total of 3 are known: Hayden et al. (1997) and Flamant et al. (1997) used the largest negative peak of the first derivative of the lidar signal as a marker for the instantaneous MLD. Menut et al. (1999) compared the absolute minimum of the second derivative of the lidar signal with the maximum of the standard deviation profile of the signal and found that the latter method overestimated the MLD when compared to radiosoundings. In a similar way, Senff et al. (1996) used profiles of the derivative of logarithm of the lidar signal. Steyn et al. (1999) fitted an idealized profile to define the ML top and the transition zone depth, but Hägeli et al. (2000) found that the technique produced biased results for complex backscatter profiles. Cohn and Angevine (2000) used a wavelet-based technique providing a scale-dependent gradient locator. The results were biased by gradients in the background signal. Recently, Brooks (2003) developed an alternative approach using multiple wavelet dilatations and capable of identifying the upper and lower limits of the transition zone remaining insensitive to vertical gradients.

In the frame of the European project EARLINET (European Aerosol Research Lidar Network) (Bösenberg et al., 2001; 2003), Barcelona and 20 European lidar stations performed regular lidar measurements from May 2000 to December 2002 to provide a climatological database of the vertical and horizontal distribution of aerosols over Europe. Among other subjects, the network studied the aerosol properties in the lower troposphere and more particularly in the ABL at different time scales (diurnal and seasonal cycle). In this context, the MLD was one of the major parameters to be retrieved. Under the rather different conditions of the EARLINET stations, most reasonable

suggestions pointed out the use of the 3 derivative methods. They can be applied to individual lidar profiles as well as to averaged lidar profiles. This fact is of importance when the signal-to-noise ratio is not high enough or if one wants to reduce data flow (in both cases, temporal averaging is required) (Menut et al., 1999).

The objective of the paper is to extract the best of these three methods and to establish the criteria necessary for its application in order to extract a MLD climatology. It is organized as follows: the lidar system, the pre-processing of the measurements made in the frame of EARLINET and the methods are presented in Section 2. In section 3.1 the lidar-derived MLD's are compared to objective radiosounding retrievals in order to find the best proxy value. Section 3.2 discusses some typical cases together with complementary data pointing out the criteria of application and the limitations of the methods. In Section 3.3, the results from the whole database are presented and discussed.

2. DATA AND METHODS

2.1. Lidar data and EARLINET

A transportable, steereable lidar system allowing three-dimensional scans has been developed at the Universitat Politècnica de Catalunya (UPC) (Rocadenbosch et al., 2002). The present system is based on a Nd:YAG laser working at the 1064-nm fundamental wavelength and at the 532-nm second harmonic, delivering pulses of equal energy (160 mJ) and 6-ns duration with a 20 Hz pulse repetition frequency (PRF). The photoreceiver is based on an avalanche photodiode (APD) with a wide spectral response (its quantum efficiency is about the same at both wavelengths). The wavelength is changed by placing manually the corresponding interference filter in front of the APD. The emission and reception axes are different so that a blind zone is observed between 0 and 250 m. However, the overlap factor reaches 1 rapidly.

In the frame of EARLINET, regular lidar measurements were undertaken from May 2000 to December 2002 on preselected dates regardless of the weather conditions (Bösenberg et al., 2001;

2003). For this reason a common schedule of three measurements per week was agreed. Measurements were performed on Mondays at 1400 LST (local standard time) +/- 1 hour and at sunset –2/+3 hour and on Thursdays at sunset –2/+3 hour. Furthermore, the network performed diurnal cycle measurements under unperturbed weather conditions, ideally under high-pressure systems to allow simultaneous observations at different stations and quantify the behaviour of aerosols at the regional scale.

All lidar measurements were made at the UPC campus, south west of Barcelona (41.39 N, 2.12 E, 115 m above sea level) at the wavelength of 532 or 1064 nm. Sequences of 1-minute duration (1200 shots) were recorded. In this analysis, X-minute integrated profiles refer to the average of X consecutive 1-minute profiles. In Section 2, for the methods' validation, X = 15 min for optimizing the matching time between lidar and radiosoundings measurements and reducing the difference that could arise by integrating lidar profiles for too long. In Section 3, in order to comply with the EARLINET rules and reduce the quantity of data, the EARLINET database was processed with X = 30 min.

2.2. Methods used in the determination of the MLD from lidar data

The optical power measured by a lidar is proportional to the signal backscattered by particles and molecules present in the atmosphere. The lidar signal can be expressed as:

$$S(r) = \frac{K}{r^2}\left[\beta^a(r) + \beta^m(r)\right]T(r)^2 + S_0 \qquad (1)$$

where β^a and β^m are, respectively, particular and molecular backscatter coefficients, K is the system constant, T is the atmospheric transmission, r is the distance between the laser source and the target (it is also called range), and S_0 is the background signal. The range-squared-corrected signal (RSCS) is then defined as:

$$RSCS = (S - S_0)r^2 \qquad (2)$$

For the marked transition between the ML and the FT, the derivative of the signal will exhibit a strong negative peak.. The MLD can be identified by the absolute minimum. The first of the three derivative methods used to estimate the MLD is the gradient method (GM). It looks for the altitude (h_{GM}) of the absolute negative minimum of the first derivative of the RSCS.

$$h_{GM} = \min\left[\frac{\partial RSCS}{\partial r}\right] \tag{3}$$

However, in complex profiles several minima exist over an extended height range and the absolute minimum does not always give the MLD but the height of the top of an upper layer. In the morning, it becomes necessary to distinguish between the newly developed ML and the residual layer (RL) from the day before. When both the ML and the RL on top of it may exist, these layers are typically well disconnected and 2 local negative minima (i.e. the first derivative crosses the x=0 axis between them) can be observed. This two-layer effect is described by Stull (1988). In other frequent situations over Barcelona, one or more layers of advected aerosols can be found on top of the ML. In all these cases, if several layers that are separated (i.e. the first derivative crosses the x=0 axis) exist, only the lowest layer is labelled ML. The difficulty is then to determine the lowest negative peak. Since RSCS is noisy, especially when reaching the MLD, the derivative of the RSCS can present several small negative peaks. A criterion to eliminate non-significant peak is to define a transition zone for every peak and compare it to a minimum depth. The depth of this zone is the height difference between the highest and the lowest data point. A peak is considered representative if its associated transition zone includes a minimum of 5 points.

The inflection point method (IPM) looks for the altitude, h_{IPM}, where the inflection point of the first derivative occurs. While Menut et al. (1999) used the absolute minimum of the second derivative, h_{IPM} corresponds to the minimum of the second derivative of the RSCS located just below h_{GM}.

$$h_{IPM} = \min\left[\frac{\partial^2 RSCS}{\partial r^2}\right] \tag{4}$$

It is important to note that so defined h_{IPM} is not independent of h_{GM} unless the GM fails. In that case, h_{IPM} corresponds to the lowest negative peak of the second derivative. The criteria that h_{IPM}

must be below h_{GM} (when the GM detects correctly the "real" transition zone between the ML and the FT) comes from the fact that the second derivative of RSCS is a function changing sign each time the first derivative of RSC changes direction. Consequently, the second derivative of RSCS tends to cross more times the x = 0 axis than its first derivative, hence complicating the search of a minimum.

The derivative of the logarithm of RSCS is proportional to the aerosol extinction gradient and therefore it can also be used to detect the largest negative gradient. The logarithm gradient method (LGM), consists in finding the altitude, h_{LGM}, at which the minimum of the first derivative of the logarithm of the RSCS is reached.

$$h_{LGM} = \min\left[\frac{\partial \ln(RSCS)}{\partial r}\right] \tag{5}$$

2.3. Radiosoundings

Everyday the Meteorological Service of Catalonia performs two radiosoundings at 0000 and 1200 UTC from the Department of Astronomy and Meteorology of the University of Barcelona, at less than 500 m from the lidar station. Given its ascent rate (4 - 8 m s^{-1}), the balloon is considered to reach the ML top in less than 3 min. At 1200 UTC, the lidar 30-minute integrated profiles show differences against 5-minute and 15-minute integrated profiles. Since the incertitude on the hour of the radiosounding launches is not negligible, an analysis of the 5-minute integrated profiles could lead to large errors in the comparison with the radiosoundings due to not-matching measurement times. Therefore, 15-minute integrated lidar profiles with starting times around 1200 UTC were chosen as a good compromise for comparison with available radiosoundings.

The bulk Richardson number method can be used both in convective conditions and in mechanical turbulence. The Richardson number, R_{ib}, is calculated as a function of altitude z as:

$$R_{ib}(z) = \frac{g(z - z_0)}{\theta(z)} \frac{[\theta(z) - \theta(z_0)]}{u(z)^2 + v(z)^2} \tag{6}$$

where g is the acceleration due to gravity, z_0 the height of the surface, θ the potential temperature, and u and v the zonal and meridian wind components, respectively. The MLD is defined as the height where the Richardson number becomes equal or larger than the so-called critical bulk Richardson number, R_{ibc}, i.e. where $R_{ib} > R_{ibc}$. A value of 0.21 is taken for R_{ibc} (Vogelezang and Holtslag, 1996; Menut et al., 1999). Beyond this critical value of R_{ib} the atmosphere can be considered fully decoupled from the ML.

For the same time period (May 2000 – December 2002), Sicard et al. (2003) compared the Richardson method with the simple parcel method (Holzworth, 1967) and found that the agreement was very good even though the simple parcel method gave slightly lower heights due to its limitations in situations dominated by mechanical turbulence. Thus, lidar profiles were compared to the MLD retrieved by the Richardson number method.

3. RESULTS AND DISCUSSION

3.1. Comparison of the MLD retrievals from lidar measurements and the Richardson number method

From the measurement period, 29 simultaneous radiosoundings and lidar measurements are available. Finally 20 lidar profiles were processed by the three analysis methods. The reasons for discarding the other 9 cases are the following:

- Cumulus clouds with little vertical extent and seemingly flattened have formed at the ML top,
- The MLD is underneath the useful lidar signal (before the overlap reaches 1),
- One of the methods exhibits too many negative peaks without crossing the x = 0 axis,
- Aerosol layer on top of the ML coupled with the ML.

Cloud screening was applied to all of the 1-minute integrated profiles by discarding the profiles featuring a positive gradient larger than a given threshold. In some cases, the MLD could not be determined simply because it was below or around 300 m, which is the altitude below which the

overlap factor between the receiver field of view and the illuminated atmospheric cross section is still increasing to reach the stationary value, which distorts the RSCS profiles.

Results of the MLD comparison between lidar and radiosoundings are shown in Figure 2. The error bars on the vertical axis represents the standard deviation of the MLD's retrieved from the 15 1-minute profiles. For each of the lidar analysis methods, a good agreement was found with correlation coefficients larger than 0.960. The smallest standard deviation is found for the IPM, with a value of 82 m, whereas it is equal to 89 and 101 m, respectively, for the GM and the LGM. Both the GM and LGM retrieve higher MLD than the IPM, which is normal since the inflexion point of the first derivative is found just before its minimum (for the LGM, this is also true: only the distances change, not the relative position of the points between each other). However, the most remarkable result is that the number of points of the MLD from the radiosoundings within the error bar of the IPM is 1.5 to 2 times larger than for the GM or the LGM. Approximately two thirds of the MLD's from the radiosoundings are within the h_{IPM} error bar. In the next section, the results from the three methods are discussed, together with their criteria of application and their limitations. Finally, in Section 3.3, the whole database is processed only with the IPM.

3.2. Data process and limitations

In order to deliver a lidar ML climatology in Barcelona and to fully test the IPM identifying its advantages and limitations, the analysis was extended to all the lidar data available from May 2000 to December 2002 (162 measurement days with 660 profiles averaged over 30 minutes). We discuss the results of the three methods on two diurnal cycle measurement days (a simple winter case and a complex summer case) with complementary information such as synoptic maps, backtrajectories and radiosoundings.

Kinematic backtrajectories were calculated with version 4 of the Hybrid Single-Particle Lagrangian Integrated Trajectory model (HYSPLIT), version 4, developed by the National Oceanic and Atmospheric Administration (NOAA)'s Air Resources Laboratory (ARL) (Draxler and Hess, 1998;

Draxler and Rolph, 2003; Rolph, 2003). In the winter case, meteorological data used for trajectory computation comes from the FNL archives maintained by the ARL (available online at http://www.arl.noaa.gov/ss/transport/archives.html). The FNL data is a product of the Global Data Assimilation System (GDAS), which uses the Global spectral Medium Range Forecast model (MRF) to assimilate multiple sources of measured data and forecast meteorology. Resolution is ~190 km horizontal and 12 vertical layers on constant pressure surfaces from 1000 to 50 mbar. Because synoptic backtrajectories associated to stagnant situations do not represent the detailed movement of the air masses and mesoscale effects may not be captured by the analyses from which the trajectories are calculated, in the summer case, the meteorological data used for trajectory computation was derived from a high resolution (9 km, 29 σ-layers) numerical simulation ran with the PSU/NCAR Mesoscale Model 5 (MM5), version 3, release 4 modelling system (Dudhia, 1993; Dudhia et al., 2001). Two nested domains were selected and one-way nesting approach was used. Initialization and boundary conditions were introduced with analysis data of the AVN global model. The physics options used for the simulations were the Gayno-Seaman planetary boundary layer scheme, based on Mellor-Yamada TKE prediction (Gayno et al., 1994), the Kain-Fritsch cumulus scheme (Kain and Fritsch, 1993), the Dudhia simple ice moisture scheme and the cloud-radiation scheme.

Additional information is provided by the temporal evolution of the MLD. Indeed, to be sure to present physically meaningful results, a cross-comparison of the temporal evolution of the MLD was made. This means that after the first evaluation of the MLD, the plots of Figures 3d and 5d are generated to check the temporal consistency between successive heights.

On 16 October 2000 the Azores high extended over the Atlantic Ocean southwest from the IP (Figure 3a). The Barcelona area was influenced by the southern edge of a low pressure system located over the north Atlantic inducing W-NW flows (see backtrajectories in Figure 3b and radiosounding in Figure 3c). The 1-minute resolution diurnal cycle which is shown in Figure 3d depicts the ML development from 0830 to 1800 UTC. Some thin clouds are observed on top of the ML just before noon (dark red spot). A thick elevated layer of 2 to 3 km depth is detected by the

lidar at an altitude of 5 km in the morning and 3 km in the afternoon. Backtrajectory analysis clearly identifies the Saharan origin of the upper air-masses. Saharan dust layers reach the northeastern IP predominantly by depressions located to the west or southwest of the IP or when the north African anticyclone shifts to the east or southeast of the IP or by the combination of both cyclone and anticyclone systems (Rodriguez et al., 2001; Pérez et al., 2003). This case is an unusual Saharan dust intrusion into the Barcelona free troposphere. Nevertheless, the diurnal cycle (Figure 3d) shows the typical winter ML development over the area under W-NW flows. The absolute minimum of the first derivative detects the "real" transition zone between the ML and the FT in all cases, hence the first criterion can be used: the MLD corresponding to h_{IPM} is given by the minimum of the second derivative just below h_{GM}. To illustrate this case, we chose to plot in Figure 4a the 30-minute RSCS profile, together with the profiles from the 3 derivative methods between 1202 and 1231 UTC. There is absolutely no ambiguity on the retrieval of h_{GM} and therefore neither on h_{IPM}. Figure 4b shows the 15-minute RSCS between 1202 and 1216 UTC. The MLD's retrieved by the three methods are reported on the figure: h_{GM} = 1111 m, h_{IPM} = 1093 m and h_{LGM} = 1123 m while the radiosounding delivers a MLD of 1084 m at 1200 UTC. The temporal variation of the signal within the ML due to the shorter time scale of the convective motions highlights the drawback of the integration time on the MLD retrieval accuracy. Within 30 minutes the instantaneous MLD can change significantly as the difference between Figure 4a and 4b shows: integrating over 30 minutes instead of 15 minutes lowers the MLD of about 40 to 50 m on average.

We now turn into a complex situation as an example of the difficulties that often appear when the previous methods are applied to the Barcelona lidar profiles. For the 30 May 2002 (Figures 5 and 6), the mean sea-level pressure map at 1800 UTC (Figure 5a) features the influence of the southern edge of a high pressure system located over western Europe inducing weak pressure gradient conditions over the region, and the formation of the typical Iberian thermal low with its corresponding relative high pressure area above the Western Mediterranean Basin (WMB). The air masses arriving at low levels at 1200 UTC had previously circulated anticiclonally over the WMB, while the upper levels

showed a peninsular origin. The 284 -m AGL backtrajectory captures the sea breeze flows over the coast Arrival directions of the backtrajectories are confirmed by the radiosounding in Figure 5c: S-SW sea-breeze flows up to 600m and SW-W flows from 600 to 4000m. Under such sea breeze conditions, a TIBL may be formed as previously observed by Soriano et al. (2001). The wind profile of the radiosounding and the 984 -m AGL backtrajectory at 1200 UTC show that the dense aerosol layer observed at about 1000m (see 1-minute resolution diurnal cycle of the RSCS in figure 5d) in the morning comes from the WMB. Relative humidity values (Figure 5c) correlate very well with the layers detected by the lidar. Humidity effects can be important on the lidar data through a swelling of the aerosols and an increase of its effective cross-section. Figures 6a, 6c and 6d show the 30-minute RSCS profiles, together with the profiles from the 3 derivative methods at 1139, 1222, and 1543 UTC, respectively. Each profile shows a multi-layer structure below 1500m. Figure 6a depicts the results at 1139 UTC. The absolute minimum of the first derivative fails and detects the top of the elevated layer at 923 m. The inversion of the upper layer has a sharper signal decrease. In this case, we use the second criterion: the MLD (at 630 m) is given by the minimum of the second derivative below the lowest negative peak of the first derivative. This is confirmed by the radiosounding (Figure 5c). Figure 6b shows the 15-minute RSCS between 1154-1208 UTC. The MLD's retrieved by the three methods are reported on the figure: h_{GM} = 725 m, h_{IPM} = 704 m and h_{LGM} = 735 m while the radiosounding delivers a MLD of 703 m at 1200 UTC. As for Figures 4a and 4b, note that integrating over 30 minutes instead of 15 minutes lowers the MLD of about 60 m. At 1222 UTC (Figure 6c), the absolute minimum of the first derivative also fails. The lowest negative peak of the first derivative leads to h_{GM} = 736 m and therefore to h_{IPM} just below at 704 m. However the largest negative peak of the second derivative would have led to a MLD of 561 m. The sequence from 1222 to 1251 UTC zoomed in Figure 5d seems to be split in 2: a first group of profiles with a transition at around 725 m, and a second group with a transition around 600 m. The IPM only detects an "averaged" height (704 m) from the 30-minute integrated profile which is closer to 725 m than 600 m. The first group of profiles (1222-1236 UTC) features a sharper signal

decrease around 725 m than the second one (1237–1251 UTC) around 600 m. While the first group can be interpreted as the core of a rising thermal penetrating into the capping inversion, the second group could be a result of down mixing of FT air into the ML. Downdrafts are in general less clearly defined, because they are not directly buoyantly driven. In these downdraft regions, the detected MLD is lower and the transition zone is wider than in the adjacent updrafts. Again, this case shows the drawback of the integration time in the ML retrieval accuracy. At 1543 UTC (Figure 6d), the upper layer is almost completely coupled to the ML and even showing higher RSCS values, but a first small decrease in the RSCS still allows the detection of the MLD (524 m) as being the minimum of the second derivative just below the lowest negative peak of the first derivative. The top of the upper layer is located at 832 m. In the climatological context, if we had considered a single 30-minute measurement, one could have stated that the MLD is located at 832 m (the inflection point just below the absolute minimum of the first derivative) arguing that the lowest negative peak of the first derivative could be attributed to inhomogeneities within the ML. This situation points out the importance of following the temporal evolution of the ML along the day. Thus, the diurnal cycle (Figure 5d) allows following the connection between the ML and the upper layer, and locating the proper minimum.

Finally, independently from the season, some multi-layer cases due to Saharan dust intrusion or re-circulation of pollutants could not be solved by neither of the methods because the ML were fully connected to the upper layer. In these cases, the GM and LGM detected the top of the first disconnected layer (usually much higher than the "real" transition zone); and the IPM detected the lowest negative peak at an altitude lower than h_{GM} corresponding to an inflexion point of the first derivative while it is positively decreasing. Even though in some cases the gradient of the signal weakened around h_{IPM}, no conclusion could be drawn only from the lidar profiles. In these cases, not even the third criterion (if GM fails, h_{IPM} corresponds to the lowest negative peak of the second derivative) could be used. These cases are unsolved cases by analysing lidar profiles from RSCS only. Considering these results and the comments from Section 1, the IPM is applied to the whole

database to retrieve the MLD.

3.3 Mixed layer depth in Barcelona between 2000 and 2002

Among the 660 measurements over 162 days, a comparison of the retrieved MLD's was made for a certain portion of the diurnal cycle. The period of maximum insolation running from 1000 to 1500 UTC was chosen, which corresponds to the unstable thermal stratification. Figure 7 shows the MLD in Barcelona retrieved by the IPM over the period May 2000 - December 2002. Two seasons are distinguished: summer (from April to September) and winter (from October to March). The MLD oscillates between 300 and 1450 m in summer and between 390 and 1420 m in winter. The standard deviation for this portion of the day is 180 and 256 m, respectively in summer and winter. Within the frame of EARLINET (Bösenberg et al., 2003), most stations showed a clear annual cycle with higher values in summer than in winter. For example, in Hamburg it has been shown that on average this cycle follows quite well a sinus function with maximum values in the beginning of July and lowest values in the beginning of January (Matthias and Bösenberg, 2002). In Figure 7, no significant differences are observed between summer and winter, even though higher values could be expected in summer. This was also the case of Athens (Greece) and Lecce (Italy) which are also coastal stations. Furthermore, in Barcelona the average MLD in summer is even smaller than the average MLD in winter. The limited growth of the ML in summer is partly caused by the amplified compensatory subsidence over the Mediterranean sea and its coastal areas, attributable to the combined sea-breeze and upslope flows plus the formation of the Iberian thermal low over the Central plateau (Millán et al., 1992; 1997). Generalized subsidence due to the Azores anticyclone and compensatory subsidence from the Iberian thermal low over the WMB represent the synoptic and large mesoscale phenomena that may explain the small growth of the ML. Millán et al. (1992; 1997) have documented the first rapid rise of the MLD during the morning followed by the sinking of its capping inversion during the afternoon. Lidar profiles in Figure 6 follow this pattern. Additionally, sea breezes introduce cool and stable air over the coast. As the column of air advects

downwind and warms, the temperature difference between the air and the ground lessens. As a result, the heat flux at the ground decreases, the ML warms less rapidly, and the rise rate of the MLD is reduced (Stull, 1988). Generally, TIBL's do not extend all the way to the top of the marine air associated with the intruding air mass, so the remainder of the cool air mass above the TIBL and below the return flows acts as well as a barrier for the TIBL vertical development. The TIBL deepens with distances downwind of the shoreline: in our case the retrieved MLD's are referred to a point located at about 5 km from the shore.

4. CONCLUSIONS

The EARLINET climatological database has been thoroughly analyzed in terms of MLD's determination in Barcelona using three derivative methods (gradient method, inflection point method and logarithm gradient method) applicable to single lidar profiles. The methods are based on the determination of the strongest negative gradient of the backscattered lidar signal. The IPM gives the best results when comparing with the Richardson number method, which is widely used to estimate MLD's from radiosoundings. The two other methods give slightly higher MLD's. To estimate h_{IPM}, three criteria were adopted: (1) if the absolute minimum of the first derivative detects correctly the "real" transition zone, h_{IPM} is the lowest negative peak of the second derivative below the absolute minimum of the first derivative; (2) if the absolute minimum of the first derivative does not detect correctly the "real" transition zone, h_{IPM} is the lowest negative peak of the second derivative below the lowest negative peak of the first derivative; (3) if GM fails, h_{IPM} is the lowest negative peak of the second derivative. It stands out from these criteria that to be able to judge for the correctness of the "real" transition zone detected by the GM, additional information is needed. Therefore, if possible one should (1) use complementary data such as synoptic maps, backtrajectories and radiosoundings, and (2) cross-compare the MLD's found with the temporal evolution of the MLD (only lidar data are needed for that). These new contributions help to overcome most of the ambiguities found.

Limitations of the IPM are found in the presence of elevated aerosol layers whenever the inversion capping of the mixed layer is weak. In these cases, small or inexistent aerosol gradients between the ML and the upper layer are much harder to detect than those from the elevated layers, which exhibit large aerosol and humidity gradients with respect to their surrounding. Layering is a recurrent pattern in Barcelona. Under strong insolation and weak synoptic forcing, sea breezes and mountain-induced winds develop to create re-circulations of pollutants along the coast. Layers are formed when aerosols are injected from the mountains into the return flow at various heights and distances from the coast. Synoptic maps and backtrajectories are essential to understand the meteorological context that can support advective transport or past accumulation processes. Single lidar analysis can introduce large biases in the MLD determination. Diurnal cycle measurements are strongly required. The retrieval methods of the MLD cannot be automated because the cross-comparison of the temporal evolution of the MLD is a key aspect of its retrieval: it guarantees temporal coherency between successive MLD's. The MLD of reference given by one radiosounding (or more) helps in validating the correctness of the temporal evolution of the MLD.

Around noon, the ML changes quite rapidly and the analysis of 30-minute integrated profiles sometimes shows large differences against 5-minute and 15-minute integrated profiles. This highlights the drawback of the integration time on the MLD retrieval accuracy: the IPM will only detect a "temporal averaged" height. The MLD cross-comparison between lidar and radiosounding measurements among all the inter-compared methods may well be influenced by atmospheric decorrelating effects taking place over the 30-minute lidar integration time, particularly between 1000 and 1500 UTC, when the boundary layer has a stronger evolution. Thus, it is necessary that the methodological analysis includes a "discard" procedure to cope with time-punctual specific uncorrelated scenes, such as those arising in cases where an aerosol layer is coupled to the ML on top of it. A methodological hint arising from Section 3.2 is to increase the correlation coefficient of the MLD cross-comparison by the temporal variance computed over the 30-minute integrated

profiles, since temporal decorrelation of the MLD is a major error source in some of the analyzed profiles.

Among the 660 measurements made over 162 days, the MLD during the period of maximum insolation (from 1000 to 1500 UTC) oscillated between 300 and 1450 m in summer and between 390 and 1420 m in winter, statistically. The standard deviation is 180 and 256 m, respectively in summer and winter. In summer, low values (mainly limited to 400-800 m ASL) are associated to compensatory subsidence over the Mediterranean sea and to the TIBL formation: the cool sea breeze entrance limits the vertical growth of the TIBL that grows with distances downwind from the coastline. There is a significant differential trend as compared to other continental European cities such as Paris or Hamburg (Bösenberg and Matthias, 2003). The analysis of complex patterns such as those occurring in Barcelona requires a progressive incorporation of new methodologies to the already existing ones along the points suggested in the examples presented in this work.

ACKNOWLEDGEMENTS

The authors thank Prof. Comerón for his valuable comments. They wish to acknowledge the following entities for partially supporting the research work and lidar systems developed at UPC: European Union under the EARLINET contract EU EVR1-CT-1999-40003, and MCYT (Spanish Ministry of Science and Technology) under the grant REN2003-09753-CO2-02. ESA and MCYT are also thanked respectively for the external postdoctoral fellowship and the *Ramón y Cajal* position hold by M. Sicard.

REFERENCES

Barros, N., Toll, I., Soriano, C., Jiménez, P., Borrego, C., and Baldasano, J. M.: 2003, 'Urban Photochemical Pollution in the Iberian Peninsula: the Lisbon and Barcelona Airsheds', *J. Air & Waste Manag. Assoc.* **53**, 347-359.

Boers, R., Spinhirne, J. D., and Hart, W. D.: 1988, 'Lidar observations of the fine-scale variability of marine stratocumulus clouds', *J. Appl. Meteorol*. **27**, 797-810.

Bösenberg, J., Ansmann, A., Baldasano, J. M., Balis, D., Böckmann, C., Calpini, B., Chaikovsky, A., Flamant, P., Hagard, A., Mitev, V., Papayannis, A., Pelon, J., Resendes, D., Schneider, J., Spinelli, N., Trickl, T., Vaughan, G., Visconti, G., and Wiegner, M.: 2001, 'EARLINET: A European aerosol research lidar network', in A. Dabas, C. Loth, J. Pelon (eds.), *Advances in Laser Remote Sensing – Selected papers presented at the 20th ILRC*, Vichy (France), July 10-14, 2000, Ecole Polytechnique, Palaiseau, France, pp. 155-158.

Bösenberg, J., and Matthias, V.: 2003, 'EARLINET: A European Aerosol Research Lidar Network to Establish an Aerosol Climatology', in *Final report for the period February 2000 to February 2003*, Max-Planck-Institut für Meteorologie, Hamburg, Germany, 212 pp.

Brooks, I. M.: 2003, 'Finding Boundary Layer Top: Application of a Wavelet Covariance Transform to Lidar Backscatter Profiles', *J. Atmos. Oceanic Technol.* **20**, 1092-1105.

Cohn, S. A., and Angevine, W. M.: 2000, 'Boundary-layer height and entrainement zone thickness measured by lidars and wind profiling radars', *J. Appl. Meteorol*. **29**, 1233-1247.

Deardorff, J. W., Willis, G. E., and Stockton, B. H.: 1980, 'Laboratory Studies of the Entrainment Zone of a Convectively Mixed Layer', *J. Fluid. Mech.* **100**, 41–64.

Draxler, R.R., and Hess, G.D.: 1998, 'An overview of the Hysplit_4 modelling system for trajectories, dispersion, and deposition', *Australian Meteorological Magazine* **47**, 295-308.

Draxler, R. R., and Rolph, G. D.: 2003, *HYSPLIT (HYbrid Single-Particle Lagrangian Integrated Trajectory) Model access via NOAA ARL READY Website (http://www.arl.noaa.gov/ready/hysplit4.html)*, NOAA Air Resources Laboratory, Silver Spring, MD.

Dudhia, J.: 1993, 'A non-hydrostatic version of the Penn State-NCAR mesoscale model: Validation tests and simulation of an Atlantic cyclone and cold front', *Monthly Weather Review* **121**, 1493-1513.

Dudhia, J., Gill, D., Guo, Y., Manning, K., and Wang W.: 2001, *PSU/NCAR Mesoscale Modeling System Tutorial Class Notes and User's Guide: MM5 Modeling System Version 3*, Mesoscale and Microscale Meteorology Division, National Center for Atmospheric Research, Boulder, CO (June 18, 2001), http://www.mmm.ucar.edu/mm5/.

Dupont, E.: 1991, *Etude méthédologique et expérimentale de la couche limite atmosphérique par télédétection laser*, Ph.D. dissertation., Université Pierre et Marie Curie, Paris, France, 220 pp.

Flamant, C., Pelon, J., Flamant, P. H., and Durand, P.: 1997, 'Lidar determination of the entrainement zone thickness at the top of the unstable marin atmospheric boundary-layer', *Boundary-Layer Meteorol.* **83**, 247-284.

Gayno, G. A., Seaman, N. L., Lario, A. M., and Stauffer, D. R.: 1994, 'Forecasting visibility using a 1.5-order closure boundary layer scheme in a 12-km nonhydrostatic model', in: *AMS Tenth Conference on Numerical Weather Prediction*, American Meteorological Society, 45 Beacon St., Boston, MA, pp. 18-20.

Hägeli, P., Steyn, D. G., and Strawbridge, K. B.: 2000, 'Spatial and Temporal Variability of Mixed-layer Depth and Entrainment Zone Thickness', *Boundary-layer Meteorol*. **97**, 47-71.

Hayden, K. L., Anlauf, K. G., Hoff, R. M., Strapp, J. W., Bottenheim, J. W., Wiebe, H. A., Froude, F. A., Martin, J. B., Steyn, D. G., and McKendry, I. G.: 1997, 'The Vertical Chemical and Meteorological Structure of the Boundary Layer in the Lower Fraser Valley during Pacific '93', *J. Atmos. Environ.* **31**, 2089–2105.

Holzworth, C. G.: 1967, 'Mixing depths, wind speeds and air pollution potential for selected locations in the United States', *J. Appl. Meteorol.* **6**, 1039-1044.

Hooper, W. P., and Eloranta, E. W.: 1986, 'Lidar measurements of wind in the planetary boundary layer: the method, accuracy and results from joint measurements with radiosonde and Kytoon', *J. Climate Appl. Meteorol.* **25**, 990-1001.

Jorba, O., Pérez, C., Rocadenbosch, F., and Baldasano, J. M.: 2004, 'Cluster analysis of 4-day backtrajectories arriving in the Barcelona area (Spain) from 1997 to 2002', *J. Appl. Meteorol*. **43**, 887-901.

Kain, J. S., and Fritsch, J. M.: 1993, 'Convective parameterisation for mesoscale models: The Kain-Fritsch scheme' in K. A. Emanuel and D. J. Raymond (eds), *The representation of cumulus convection in numerical models*, American Meteorological Society, 45 Beacon St., Boston, pp. 246.

Martín-Vide, J.: 1987, *Característiques climatològiques de la precipitació en la franja costera mediterrània de la Península Ibèrica*, PhD. Dissertation, Institut Cartogràfic de Catalunya, Barcelona, Spain, 245 pp.

Matthias, V. and Bösenberg, J.: 2002, 'Aerosol climatology for the planetary boundary layer derived from regular lidar measurements', *Atmos. Res.* **63**, 221-245.

Melfi, S. H., Spinhirne, J. D., Chou, S. H., and Palm, S. P.: 1985, 'Lidar observation of the vertically organized convection in the planetary boundary layer over the ocean', *J. Climate Appl. Meteorol.* **24**, 806-821.

Menut, L., Flamant, C., Pelon, J., and Flamant, P. H.: 1999, 'Urban boundary-layer height determination from lidar measurements over the Paris area', *Appl. Opt*. **38**, 945-954.

Millán, M. M., Artinñano, B., Alonso, L., Castro, M., Fernandez-Patier, R., and Goberna, J.: 1992, 'Mesometeorological cycles of air pollution in the Iberian Peninsula', *Air Pollution Research Report 44*, Commission of the European Communities, Brussels, Belgium, 219 pp.

Millán, M., Salvador, R. and Mantilla, E.: 1997, 'Photooxidant dynamics in the Mediterranean basin in summer: results from European research projects', *J. Geophys. Res.* **102**, 8811-8823.

Nickovic, S., Kallos, G., Papadopoulos, and A., Kakaliagou, O.: 2001, 'A model for prediction of desert dust cycle in the atmosphere', *J. Geophys. Res.* **106**, 18113–18129.

Pérez, C., Jiménez, P., Rocadenbosch, F., and Baldasano, J.M., 2003, 'Lidar observations of Saharan dust and regional pollution events over the northeastern Iberian Peninsula in the frame of

EARLINET', in *American Association for Aerosol Research 2003 – Abstract of the 22nd Annual Conference*, Anaheim, California, October 20-24, 2003, pp. 89.

Pérez, C., Sicard, M., Jorba, O., Comerón, A., and Baldasano, J. M.: 2004, 'Summertime re-circulations of air pollutants over the north-eastern Iberian coast observed from systematic EARLINET lidar measurements in Barcelona', Atmos Environ. **38**, 3983-4000.

Rocadenbosch, F., Sicard, M., Comerón, A., Baldasano, J. M., Rodríguez, A., Agishev, R., Muñoz, C., López, M. A. and García-Vizcaino, D.: 2002, 'The UPC scanning Raman lidar: an engineering overview', in L. Bissonnette, G. Roy, G. Vallée (eds.), *Lidar Remote Sensing in Atmospheric and Earth Sciences – Reviewed and revised papers presented at the 21st ILRC*, Québec (Canada), July 8-12, 2002, Defence R& D Canada – Valcartier, Val-Bélair, Canada, pp. 69-70.

Rodríguez, S., Querol, X., Alastuey, A., Kallos, G. and Kakaliagou, O.: 2001, 'Saharan dust contribution to PM10 and TSP levels in Southern and Eastern Spain', *Atmos. Environ*. **35**, 2433-2447.

Rodríguez, S., Querol, X., Alastuey, and A., Mantilla, E.: 2002, 'Origin of high summer PM10 and TSP concentrations at rural sites in eastern Spain', *Atmos. Environ.* **36**, 3101–3112.

Rolph, G. D.: 2003, *Real-time Environmental Applications and Display sYstem (READY) Website (http://www.arl.noaa.gov/ready/hysplit4.html)*, NOAA Air Resources Laboratory, Silver Spring, MD.

Seibert, P., Beyrich, F., Gryning, S. E., Joffre, S., Rasmussen, A., and Tercier, P.: 1998, 'Mixing layer depth determination for dispersion modelling', *COST Action 710 - Final Report. Harmonisation of the pre-processing of meteorological data for atmospheric dispersion models*, *Report of Working Group 2*, Office for Official Publications of the European Communities, Luxembourg, 431 pp.

Seibert, P., Beyrich, F., Gryning, S. E., Joffre, S., Ramussen, A., and Tercier, P.: 2000, 'Review and intercomparison of operational methods for the determination of hte mixing height', *Atmos. Environ.* **34**, 1001-1027.

Senff, C., Bösenberg, J., Peters, G., and Schaberl, T.: 1996, 'Remote sesing of turbulent ozone fluxes and the ozone budget in the convective boundary layer with DIAL and radar-RASS: a case study', *Contrib. Atmos. Phys.* **69**, 161-176.

Sicard, M., Pérez, C., Comerón, A., Baldasano, J. M., and Rocadenbosch, F.: 2003, 'Determination of the mixing layer height from regular lidar measurements in the Barcelona Area', in K. P. Schäfer, A. Comerón, M. R. Carleeer, and R. H. Picard, *Proc. SPIE* 5235-66, ISSN 0277-786X, ISBN 0-8194-5118-5, Barcelona, Spain, September 8-12, 2003, SPIE, PO Box 10, Bellingham, WA, pp. 505-516.

Soriano, C., Baldasano, J. M., Buttler, W. T., and Moore, K.: 2001, 'Circulatory patterns of air pollutants within the Barcelona air basin in a summertime situation: lidar and numerical approaches', *Boundary-Layer Meteorol*. **98**, 33-55.

Steyn, D. G., Baldi, M., and Hoff. R.: 1999, 'The detection of mixed layer depth from lidar backscatter profiles', *J. Atmos. Oceanic Tech.* **16**, 953-959.

Stull, R.B.: 1988, *An introduction to boundary layer meteorology*, Kluwer Academic Publishers, Dordrecht, The Netherlands, 670 pp.

Vogelezang, D. H. P., and Holtslag, A. A. M.: 1996, 'Evaluation and model impacts of alternative boundary-layer height formulations', *Boundary-Layer Meteorol*. **81**, 245-269.

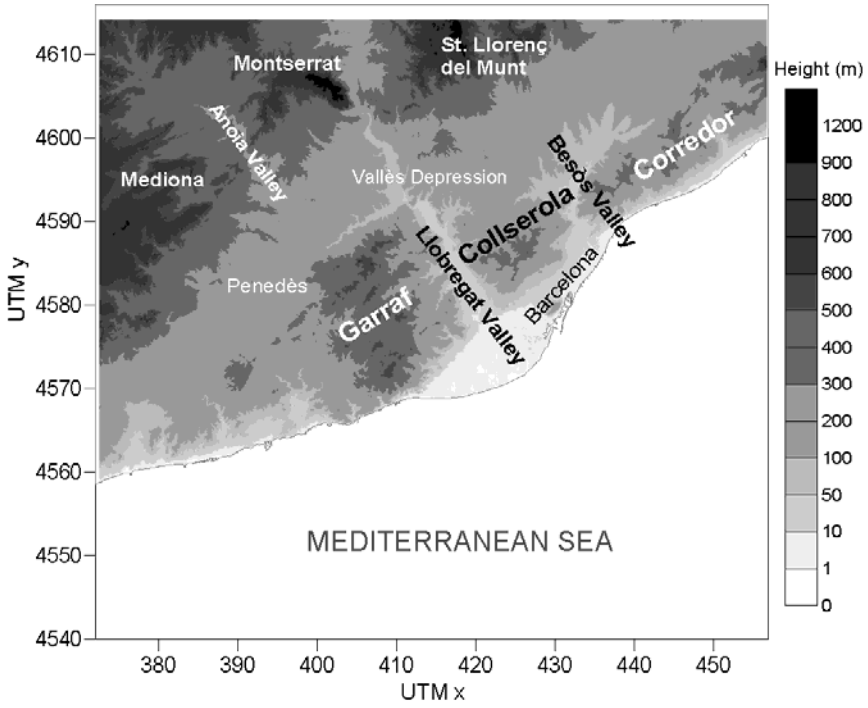

Figure 1: Orography of the Barcelona geographical area. Coastal Mountains: Garraf, Collserola and Corredor. Pre-coastal mountains: Mediona, Montserrat and St. Llorenç del Munt

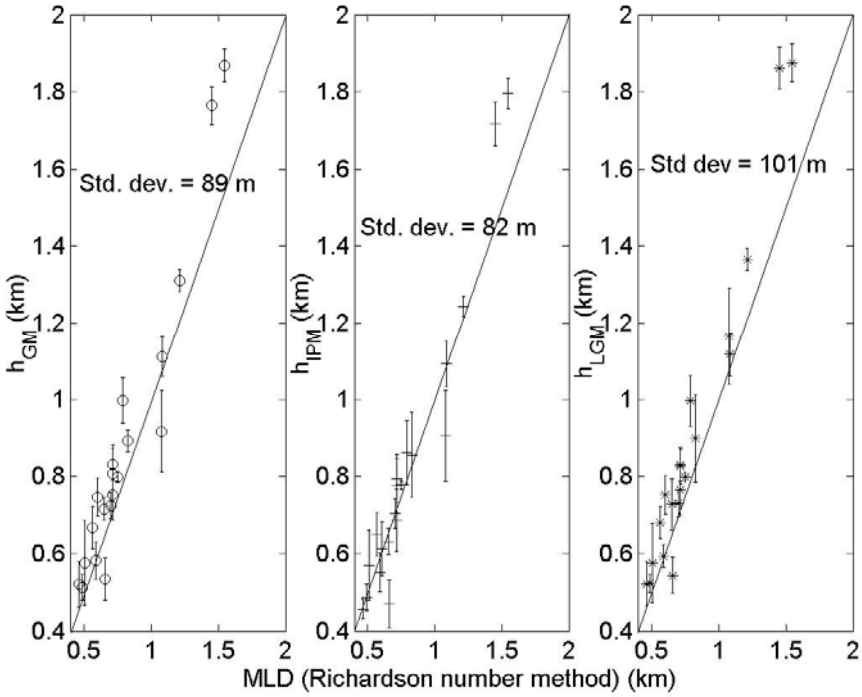

Figure 2: Comparison of h_{GM}, h_{IPM} and h_{LGM} with the MLD retrieved from radiosoundings by the Richardson number method. The standard deviation is reported in the middle of the figure for each method.

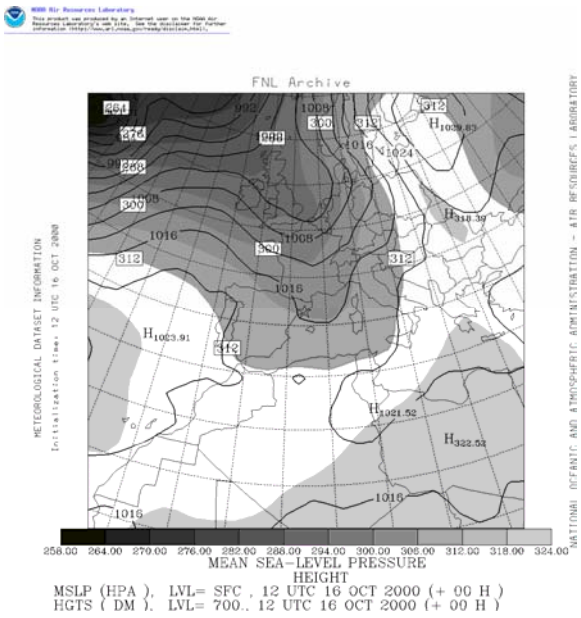

(a)

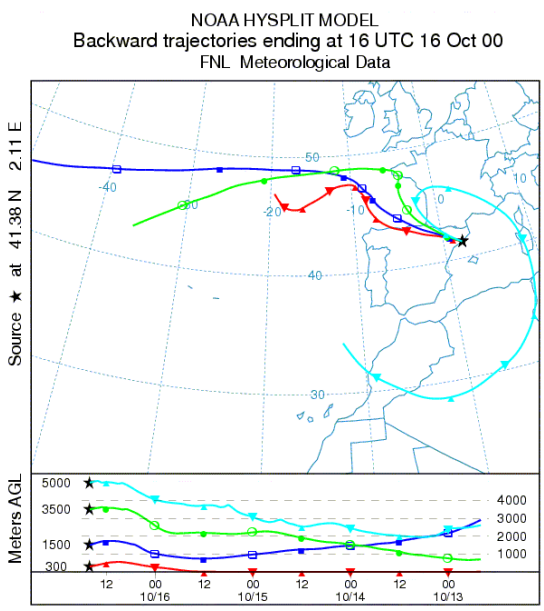

(b)

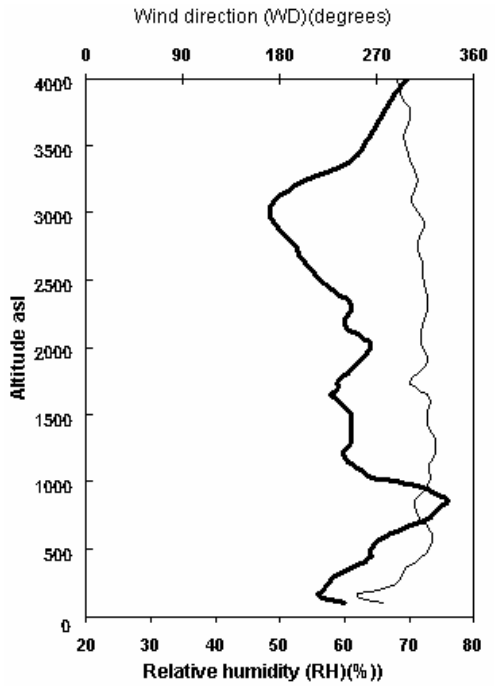

(c)

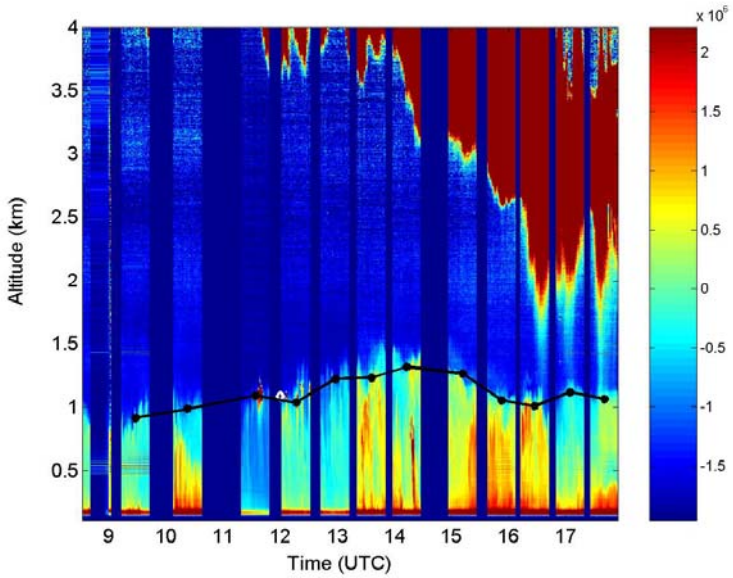

(d)

Figure 3: 16 Oct 2000: (a) MSL pressure and 700 hPa geopotential height at 1200 UTC; (b) 4-day backtrajectories arriving at 300, 1500, 3500 and 5000 m at 1600 UTC over Barcelona; (c) relative humidity (thick solid line) and wind direction (thin solid line) from the radiosounding at 1200 UTC; (d) 1-minute resolution diurnal cycle of the RSCS. The black dots indicate the MLD retrieved by the IPM. The white diamond indicates the MLD from the 1200 UTC radiosounding by the Richardson number method.

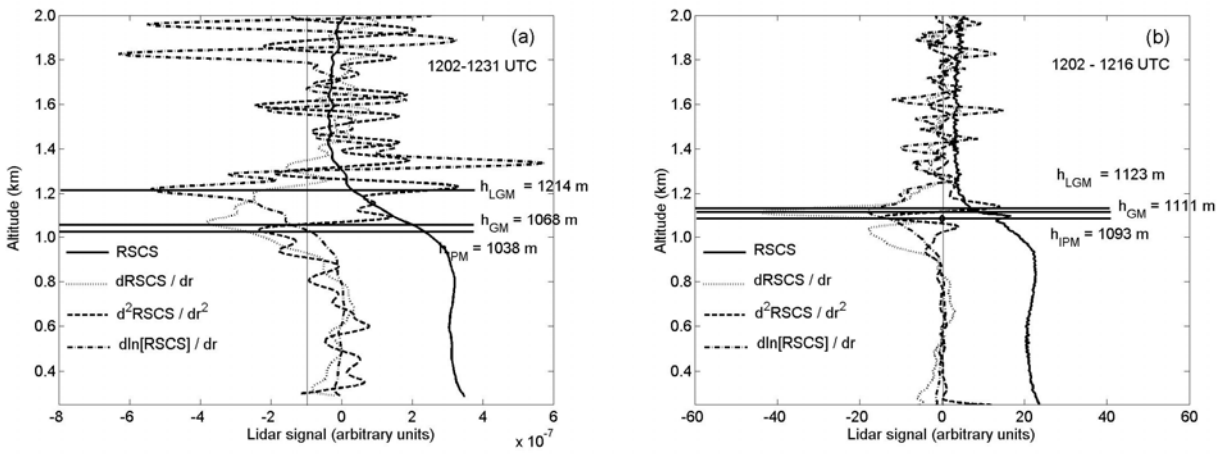

Figure 4: (a) 30-minute integrated RSCS profiles on 16 October 2000 between 1202 and 1231 UTC, and (b) 15-minute integrated RSCS profiles on 16 October 2000 between 1202 and 1216 UTC. The black diamond represents the MLD (1084 m) from the radiosounding at 1200 UTC.

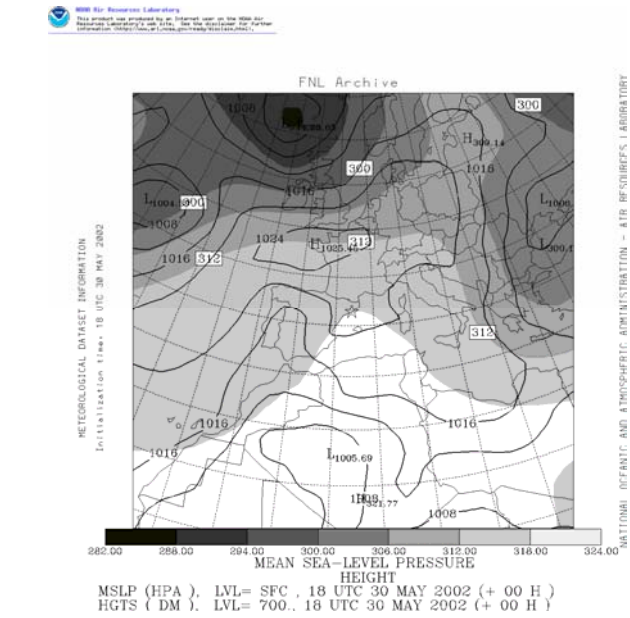

(a)

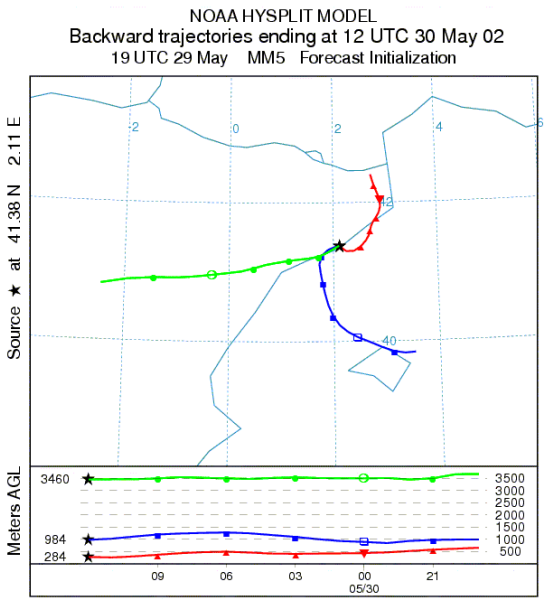

(b)

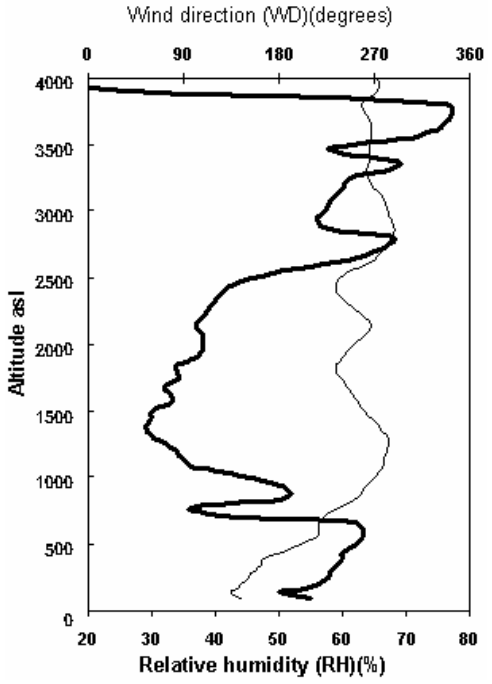

(c)

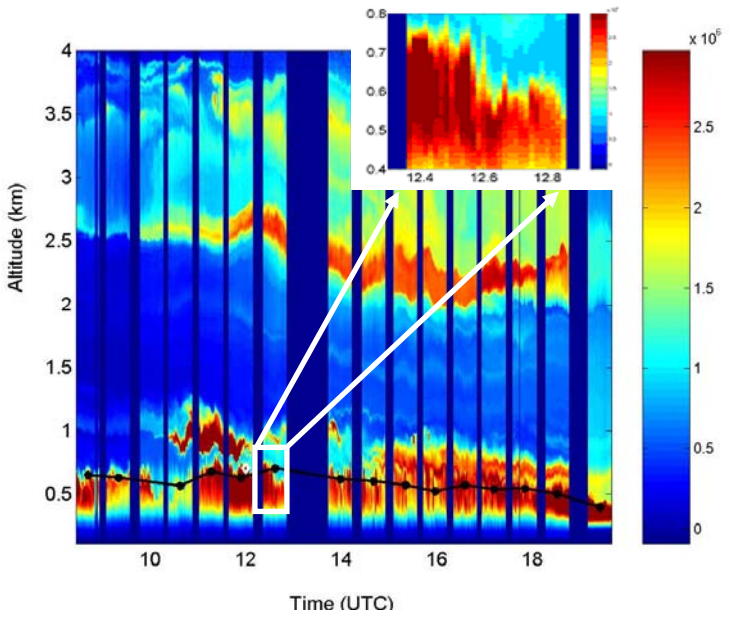

(d)

Figure 5: 30 May 2000: (a) MSL pressure and 700 hPa geopotential height at 1800 UTC; (b) 18-hour backtrajectories arriving at 284, 984 and 3460 m at 1200 UTC over Barcelona; (c) relative humidity (thick solid line) and wind direction (thin solid line) from the radiosounding at 1200 UTC; (d) 1-minute resolution diurnal cycle of the RSCS. The black dots indicate the MLD retrieved by the IPM. The white diamond indicates the MLD from the 1200 UTC radiosounding by the Richardson number method.

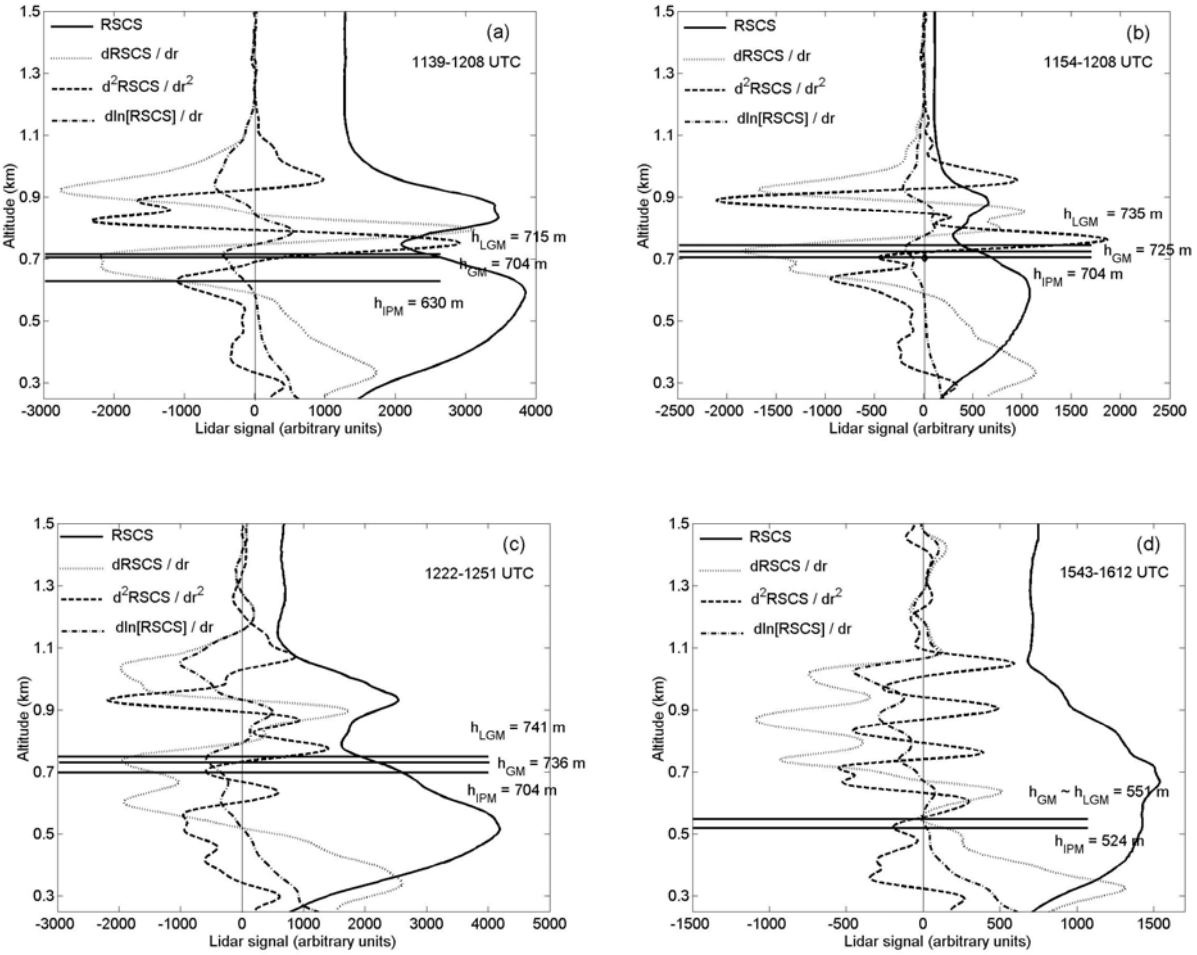

Figure 6: 30-minute integrated RSCS profiles on 30 May 2002 (a) at 1139, (c) 1222, and (d) 1543 UTC. (b) is the 15-minute integrated RSCS profiles on 16 October 2000 between 1154 and 1208 UTC. The black diamond represents the MLD (703 m) from the radiosounding at 1200 UTC.

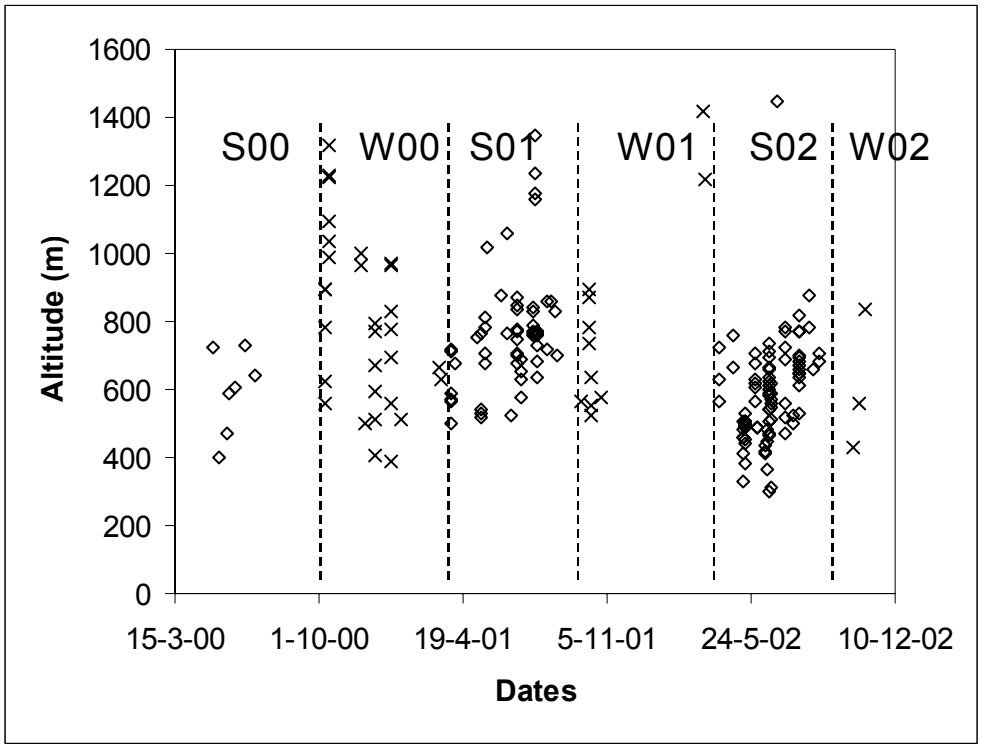

Figure 7: Mixed layer depth as a function of day of the year between May 2000 and December 2002. Diamonds indicate summer measurements (S) and crosses indicate winter measurements (W).